Predictive Model for Oxidative C–H Bond Functionalization Reactivity with 2,3-Dichloro-5,6-dicyano-1,4-benzoquinone (DDQ)

Cristian A. Morales-Rivera, Paul E. Floreancig*, and Peng Liu*

Department of Chemistry, University of Pittsburgh, Pittsburgh, Pennsylvania 15260, United States

ABSTRACT: 2,3-Dichloro-5,6-dicyano-1,4-benzoquinone (DDQ) is a highly effective reagent for promoting C–H bond functionalization. The oxidative cleavage of benzylic and allylic C–H bonds using DDQ can be coupled with an intra- or intermolecular nucleophilic addition to generate new carbon–carbon or carbon–heteroatom bonds in a wide range of substrates. The factors that control the reactivity of these reactions are well defined experimentally but the mechanistic details and the role of substituents in promoting the transformations have not been firmly established. Herein, we report a detailed computational study on the mechanism and substituent effects for DDQ-mediated oxidative C–H cleavage reactions in a variety of substrates. DFT calculations show that these reactions proceed through a hydride transfer within a charge transfer complex. Reactivity is dictated by the stability of the carbocation intermediate, the degree of charge transfer in the transition states, and, in certain cases, secondary orbital interactions between the π orbital of the forming cation and the LUMO of DDQ. A linear free energy relationship was established to offer a predictive model for reactivity of different types of C–H bonds based on the electronic properties of the substrate.

1. Introduction

Carbon–hydrogen bond functionalization reactions can greatly facilitate chemical synthesis due to their capability to increase molecular complexity from readily available starting materials with minimal waste generation.¹ These processes are most often achieved through transition metal catalysis, though metal-free approaches for such reactions are becoming increasingly common. 2,3-Dichloro-5,6-dicyano-1,4-benzoquinone (DDQ) is a mild yet effective reagent for promoting oxidative C–H bond cleavage. 2,3,4 This reagent is most commonly employed to cleave benzylic and allylic ethers through oxidative oxocarbenium ion formation followed by hydrolysis. These oxocarbenium ions can also be trapped with an intra- or intermolecular nucleophilic addition to generate carbon–carbon 3,4 (Scheme 1) and carbon–heteroatom bonds. This process is tolerant of numerous functional groups and has been used in late stages of natural product syntheses.

Scheme 1. DDQ-Mediated Intra- and Intermolecular C–C Bond Forming Reactions

a. OAC DDQ
$$Ar \rightarrow R^3$$
 $Ar \rightarrow R^3$ $Ar \rightarrow R^3$

DDQ-mediated C-H functionalization has been performed on a wide variety of substrates, with specific examples being illustrated in Scheme 2. The rates of these reactions commonly correlate with the stabilities of the intermediate carbocations. For example, benzylic C-H bond cleavages are promoted by electron-donating substituents (Scheme 2a).3a Internal allylic substrates are much more reactive than terminal allylic substrates (Scheme 2b).3a Additionally, the reactivity is significantly enhanced by the formation of aromatic carbocation intermediates, as seen in the reaction of 9 (Scheme 2c).3g Attributing the kinetics of C-H bond cleavage solely to carbocation stability, however, is inconsistent with the difference in reactivity between alkenyl and allylic ethers (Scheme 2d).7 Although alkenyl ether 13 and allylic ether 15 react with DDQ to provide the same oxocarbenium ion, the cyclization of 13 is significantly faster. This is particularly notable in consideration of the greater stability of 13 relative to 15, and indicates that substrate oxidation potential also influences reaction rates.

Clearly, a thorough understanding of the mechanisms of the DDQ-mediated C–H cleavage is necessary to elucidate the origin of reactivity. Four different mechanisms have been proposed for DDQ-mediated oxidative C–H bond cleavage reactions (Scheme 3). A single electron transfer (SET) from the substrate to DDQ can form a charge transfer complex of a radical cation with DDQ • followed by hydrogen atom transfer (HAT) to form a carbocation and a 4-hydroxyphenolate derivative (DDQH⁻). ⁸, ⁹ This mechanism is consistent with the importance of oxidation potential on the reaction rate but is not consistent with the relatively modest reduction potential of DDQ. ¹⁰ Alternatively, hydrogen atom transfer (HAT) from the substrate to DDQ can form an alkyl radical followed by single electron transfer to form the same carbocation. This mechanism, proposed by Rüchardt based on the trapping of the intermediary radicals by nitrosobenzene, ¹¹ is unlikely

Scheme 2. Experimental Reactivity Trend of Different C-H Bonds in DDQ-Mediated Oxidative Coupling Reactions^{3a,3g,7}

because the known lack of substituent effects on benzylic C–H bond strengths¹² is contrary to the observed influence of cation-stabilizing substituents on reaction rates, and kinetic isotope effects clearly show that C–H bond cleavage is the rate-determining step. ¹³ A one-step hydride transfer to the oxygen atom on DDQ (O-attack) can

directly form a zwitterionic complex of DDQH⁻ with carbocation, as proposed by Linstead and Jackman. ¹⁴ Hydride transfer to the carbon atom attached to the cyano group on DDQ (C-attack) followed by aromatization to form DDQH⁻ can generate the same carbocation. ¹⁵ The observed correlation between intermediate cation stability and reaction rate supports the direct hydride transfer mechanisms, though this pathway does not explain the observed importance of substrate oxidation potential. DFT calculations from Chan and Radom, ¹⁶ Mayr and Zipse, ¹⁵ and others ^{17, 18} suggest that the most favorable pathway in the dehydrogenation of 1,4-cyclohexadiene in polar solvent is the concerted hydride transfer via O-attack. However, the mechanism of reactions with other C–H hydride donors, including benzylic and allylic ethers, and the origin of substituent effects on rates have yet to be investigated computationally.

Scheme 3. Possible Mechanisms of DDQ-Mediated C-H Cleavage

This manuscript describes a computational study on the mechanism and origin of reactivity of a wide variety of C–H bonds in the DDQ-mediated oxidative C–C coupling reactions. The four pathways shown in Scheme 3 were analyzed computationally to elucidate the most favorable mechanism for C–H bond cleavage. A thorough theoretical analysis of the transition state interactions was then performed to reveal the main factors that dictate the reactivity. These theoretical insights and the DFT-computed barriers were utilized to establish a two-variable mathematical equation to predict the rate of the C–H cleavage from the hydride dissociation energy (HDE)¹⁹ and the oxidation potential of the substrate.

2. Computational Details

All calculations were performed with Gaussian 09.²⁰ Images of the 3D structures of molecules were generated using CYLView.²¹ The geometries of all intermediates and transition states were optimized with the M06-2X²² functional and the 6-31G(d) basis set. Single point energy calculations were performed with M06-2X and the 6-311++G(d,p) basis set. Solvent is expected to impact both the optimized geometries and the energies of the hydride transfer transition states and the zwitterionic complexes. Solvation effects were taken into account by applying the SMD²³ solvation model with 1,2-dichloroethane (DCE) solvent in both geometry optimization and single point energy calculations. Thermal corrections to the Gibbs free energies and enthalpies were calculated

using the harmonic oscillator approximation at 298K. All energies in the reaction energy profiles are with respect to the separated reactants. Each structure reported is the lowest energy conformer as indicated by calculations. Structures of higher energy conformers are provided in the Supporting Information. Oxidation potentials were calculated from the reaction Gibbs free energies of the oxidation half-reactions in DCE solution (see SI for details). ^{10c, 24} The activation free energies of the outer-sphere single electron transfer reactions were calculated from Marcus theory (see SI for details). ²⁵

3. Results and Discussion

3.1. Mechanisms of DDQ-Mediated C-H Benzylic Ether Functionalization

We first studied the single electron transfer (SET), hydrogen atom transfer (HAT), and the O- and C-attack hydride transfer pathways of the C-H cleavage step in the reaction between DDQ and benzylic ether 16. The computed activation energies and reaction energies are shown in Scheme 4. The O-attack hydride transfer is the most thermodynamically favorable pathway to form the carbocation intermediate 21 and DDOH- (22) with a reaction Gibbs free energy of –10.8 kcal/mol. The C-attack pathway to form the same carbocation 21 and the less stable nonaromatized DDQHisomer 23 is slightly endergonic by 4.6 kcal/mol. The SET and HAT pathways are all much more endergonic, with reaction Gibbs free energies of 20.7 and 13.9 kcal/mol, respectively. The activation Gibbs free energy of the SET pathway was calculated using Marcus theory (see SI for details). The barrier to the outer-sphere single electron transfer from **16** to DDQ (ΔG^{\dagger} = 22.6 kcal/mol) is higher than both the O- and C-attack hydride transfer pathways. H-atom abstraction can also be discarded because an open-shell HAT transition state cannot be located in solution. Instead, such calculations lead to the more stable closed-shell hydride transfer transition state. 26 These results indicate that the two hydride transfer pathways (O-attack and C-attack) are the most favorable mechanisms for the DDQ-mediated benzylic C-H cleavage.

The complete reaction energy profiles of the two hydride transfer pathways in the oxidative cyclization of benzylic ether 16 are shown in Figure 1A. DDQ first coordinates with 16 to form a chargetransfer complex 24. Natural population analysis (NPA) calculations show the total atomic charges of the DDQ fragment is -0.110 e (Figure 1B), indicating that complex **24** is stabilized by a small amount of charge transfer from the substrate to DDQ. From 24, the hydride from the benzylic C-H bond may be transferred to either the carbonyl oxygen on DDQ (O-attack, TS2, $\Delta G^{\dagger} = 20.5$ kcal/mol) or the cyano-substituted carbon on DDQ (C-attack, **TS1**, ΔG^{\dagger} = 19.2 kcal/mol). The C-attack pathway requires a slightly lower barrier than the O-attack pathway. This contrasts with the DDQ-mediated C-H oxidation of 1,4-cyclohexadiene, in which the O-attack is favored by 2.2 kcal/mol.¹⁵ NPA calculations revealed significant amounts of electron transfer from the substrate to DDQ in both C- and O-attack transition states (0.746 and 0.742 e in TS1 and TS2, respectively). This is consistent with the nature of the hydride transfer process. The proximity of the negatively charged DDQ and the positively charged aryl moiety of the substrate suggests that the hydride transfer transition state is stabilized by the electrostatic interactions between DDO and the benzylic ether substrate (see below for detailed discussions of factors that determine reactivity).

Scheme 4: Activation and Reaction Energies of Competing C–H Cleavage Pathways in the Reaction of DDQ and Benzylic Ether 16^a

SET RO

$$AG^{\ddagger} = 22.6$$
 $AG = 20.7$
 $AH = 24.6$

17

18

HAT RO

O'CN

OAC

 $AG = 13.9$
 $AH = 17.6$

OMe

O-attack RO

 $AG^{\ddagger} = 20.5$
 $AG = -10.8$
 $AH = -8.1$

CI CN

O'CN

OH

CI CN

O

^a All energies are in kcal/mol with respect to the separate reactants (16 and DDQ).

The C- and O-attack hydride transfer transition states lead to zwitterionic complexes of the benzylic cation with two isomers of DDQH⁻ (25 and 26, respectively). Tautomerization of the nonaromatized isomer of DDQH⁻ in 25 forms the much more stable isomeric complex 26. Dissociation of the carbocation 21 from the zwitterionic complex 26 followed by intramolecular nucleophilic addition forms a new C–C bond (27) via a cyclization transition state (TS3). This nucleophilic C–C bond formation has a lower barrier than the C–H cleavage via TS1 or TS2. Thus, the hydride transfer is the rate-determining step of the overall transformation, in agreement with the primary KIE observed in experiment. Finally, acylium ion loss from 27 will lead to the cyclic ketone product. This final step in the oxidative C–C coupling reaction is expected to be facile and exothermic, and thus was not investigated computationally.

3.2. Mechanisms of DDQ-Mediated C-H Functionalization of An Allylic Ether

We next studied the four mechanistic pathways using allylic ether ${\bf 28}$ as the substrate. The computed reaction energies of the single electron transfer (SET), hydrogen atom transfer (HAT), and two different hydride transfer pathways (O-attack and C-attack) are shown in Scheme 5. Similar to the reaction with benzylic ether ${\bf 16}$, the most thermodynamically favorable pathway is through a one-step hydride transfer to form the carbocation intermediate ${\bf 31}$ and DDQH $^-$ (${\bf 22}$). The activation free energy of the SET pathway derived from the Marcus theory is also higher than the hydride transfer pathways.

The computed energy profile of the two hydride transfer pathways in the oxidative cyclization of 28 (Figure 2A) indicated a mechanism similar to that with benzylic ether 16. DDQ first coordinates with 28 to form a charge-transfer complex 32. NPA calculations show the charge transfer from 28 to DDQ in complex 32 is slightly less significant than that in the complex with benzylic

ether (-0.062 e and -0.110 e in 32 and 24, respectively). In addition, the charge transfer in the hydride transfer transition states **TS4** and **TS5** is also less significant than that in **TS1** and **TS2**. This is consistent with the lower polarizability and higher oxidation potential of **28**. The O-attack hydride transfer (**TS4**) is favored by

1.4 kcal/mol, in contrast to the reaction with benzylic ether 16 that favors the C-attack. The carbocation resulting from the hydride transfer (31) then undergoes intramolecular nucleophilic attack (TS6) to form a new C–C bond in intermediate 35.

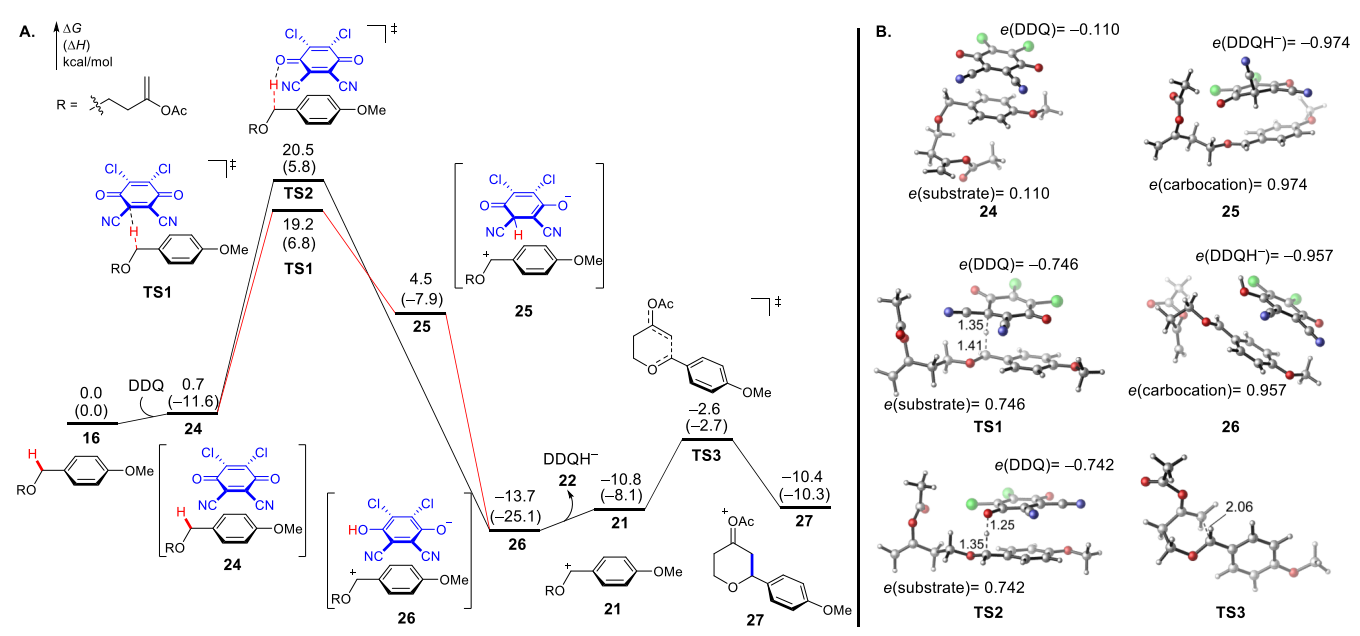


Figure 1. A. Energy profile of the DDQ-mediated intramolecular oxidative C–C coupling of benzylic ether **16**. B. 3D structures of key intermediates and transition states.

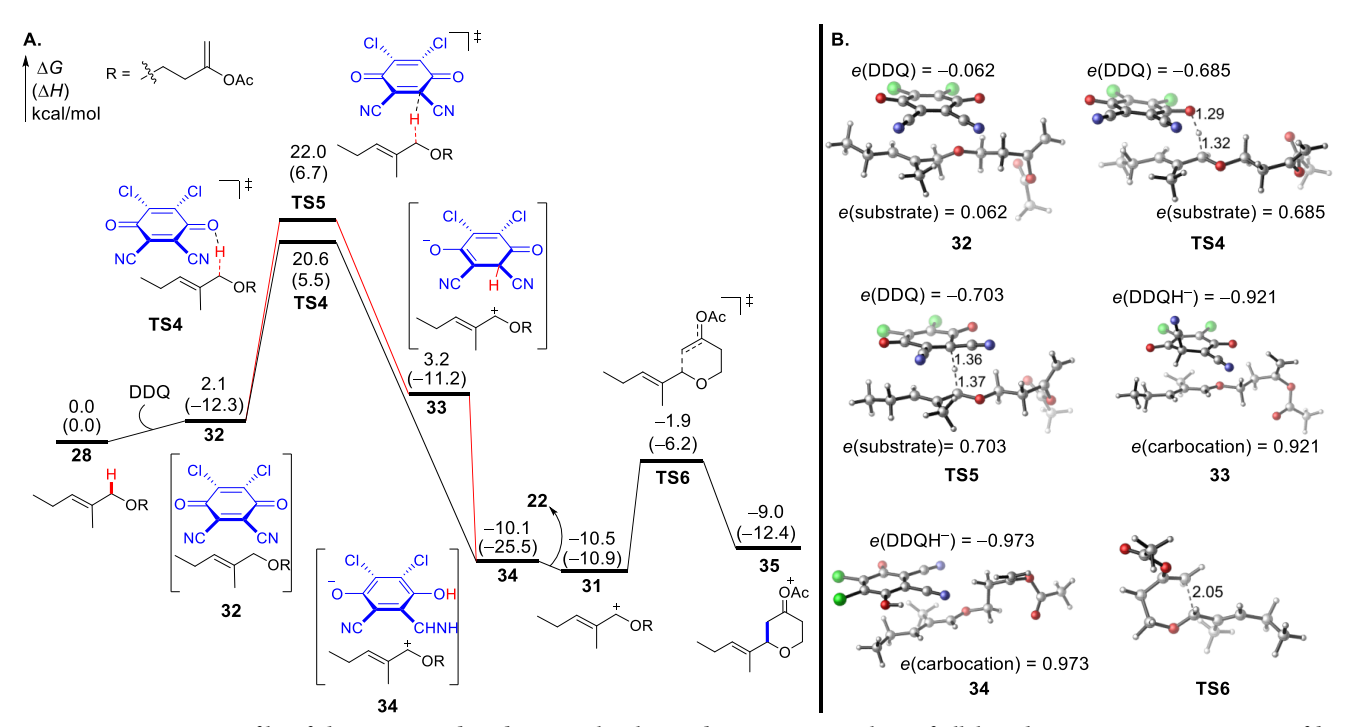


Figure 2. A. Energy profile of the DDQ-mediated intramolecular oxidative C–C coupling of allylic ether **28**. B. 3D structures of key intermediates and transition states.

Scheme 5. Activation and Reaction Energies of Competing C-H Cleavage Pathways in the Reaction of DDQ and Allylic Ether 28°

^a All energies are in kcal/mol with respect to the separate reactants (28 and DDQ).

In summary, the DFT calculations revealed that the most favorable mechanism of the DDQ-mediated C-H cleavage of benzylic and allylic ethers is a one-step hydride transfer from the charge-transfer complex of the substrate and DDQ. Two competing pathways involving hydride transfer to the oxygen and carbon atoms on DDQ, namely O- and C-attack, respectively, have similar activation energies. This indicates that both mechanisms need to be considered in the computational investigation of reactivities of different substrates.

3.3. Effects of the Stability of the Carbocation Intermediate on the Reactivity of C-H Cleavage

Activation energies of the O- and C-attack hydride transfer pathways of various benzylic ether, allylic ether, and alkenyl ether substrates were computed in order to explore the origin of substituent effects on reactivity (Table 1 and Figure 3). Even though large variations of the computed activation energies were observed among the substrates, the O- and C-attack pathways for a given substrate are always competitive. The reaction energies to generate the carbocation intermediate and DDQH- were also computed. In agreement with the experimentally observed trend, the stability of the carbocation plays an important role on the rate of the C-H bond cleavage. For example, the para-methoxy substitution stabilizes the carbocation intermediate and increases the reactivity of benzylic ether **16** compared to **36** (entries 1 and 2 in Table 1 and Scheme 2a). The reaction of internal allylic ether 28 is more exergonic and has a lower barrier than that of terminal allylic ether 37 (entries 3 and 4 in Table 1 and Scheme 2b). Forming an aromatic cation is highly thermodynamically favorable and leads to significantly increased reactivity of 9 and 38 (entries 5-7 in Table 1 and Scheme 2c). The stabilities of the intermediate carbocations are significant due to the capacity of these species to engage in bimolecular carbon-carbon bond forming reactions with allylic silanes and potassium alkenylalkynyltrifluoroborates.3g

Steric repulsions and ring strain can also destabilize the carbocation intermediate and impede hydride transfer. In the reactions shown in Figure 3A, *cis*-allylic ether **40** is less reactive than the corresponding *trans*-isomer **39** due to the unfavorable A^{1,3}-strain in carbocation **46**. This agrees with the lower reactivity of *cis* allylic ethers in experiment (Scheme 2d). The cyclic allylic ether **41** is much less reactive than the acyclic allylic ethers (**39** and **40**), because the hydride transfer to form **48** is much less exergonic. This is attributed to the increased ring strain of the cyclic allylic cation **48**. The same reactivity trend is observed for alkenyl ethers. The *trans* isomer **42** is more reactive than the *cis* isomer (**43**) and the cyclic alkenyl ether **44** is the least reactive (Figure 3B).

Table 1: Electronic Effects on the Activation and Reaction Energies of Hydride Transfer

| | DDQ , | | но | ·O 22 | | | | | | | |
|-------------------|----------------------------|---|---|---|--|--|--|--|--|--|--|
| | H _V | OR ² | NC, CN | I | | | | | | | |
| R ¹ | | -attack | • | R ¹ OR ² | | | | | | | |
| Α | , CI, | , CI] | 1 | В | | | | | | | |
| | O NC | CN CN | CI, CI | | | | | | | | |
| | DDQ R ¹ | H _{OR2} | | _ | | | | | | | |
| | | -attack | H CN CN | 23 | | | | | | | |
| O-attack C-attack | | | | | | | | | | | |
| entry | substrate | $\Delta G^{\scriptscriptstyle \dagger}$ | $\Delta G^{\scriptscriptstyle \dagger}$ | $\Delta G_{(A	o B)} \ \left[\Delta H_{(A	o B)} ight]^b$ | | | | | | | |
| | | $[\Delta H^{\dagger}]$ | $[\Delta H^{\dagger}]$ | [Δ11(A→B)] | | | | | | | |
| | OAc | | | | | | | | | | |
| 1 | | 22.9 | 23.8 | -6.8 | | | | | | | |
| 1 | | [10.7] | [10.2] | [-5.3] | | | | | | | |
| | 36 | | | | | | | | | | |
| | OAc | | | | | | | | | | |
| 2 | | 20.5 | 19.2 | -10.8 | | | | | | | |
| | MeO | [5.8] | [6.8] | [-8.1] | | | | | | | |
| | 16 | | | | | | | | | | |
| | OAc L | | | | | | | | | | |
| 3 | , , I | 26.5 | 26.1 | -4.9 | | | | | | | |
| 3 | \sim \downarrow \sim | [10.7] | [12.4] | [-5.0] | | | | | | | |
| | 37 | | | | | | | | | | |
| | OAc | 20.6 | 22.0 | 10.5 | | | | | | | |
| 4 | | [5.5] | 22.0 [6.7] | -10.5 [-10.9] | | | | | | | |
| | 28 | [3.3] | [0./] | [-10.9] | | | | | | | |
| | | | | | | | | | | | |
| 5 | | 24.9 | 25.0 | -7.4 | | | | | | | |
| 3 | н 11 | [11.1] | [11.3] | [-6.8] | | | | | | | |
| | | | | | | | | | | | |
| 6 | \ | 19.0 | 17.9 | -12.8 | | | | | | | |
| Ü | 9 ^Ĥ | [5.8] | [4.8] | [-12.2] | | | | | | | |
| | , | | | | | | | | | | |
| 7 | | 18.6 | 20.4 | -15.2 | | | | | | | |
| , | 38 | [4.7] | [7.0] | [-15.0] | | | | | | | |
| | | | | | | | | | | | |

^a All energies are in kcal/mol with respect to the separate reactants (**A** and DDQ). ^b The reaction energy of **A** and DDQ to form **B** and **22**.

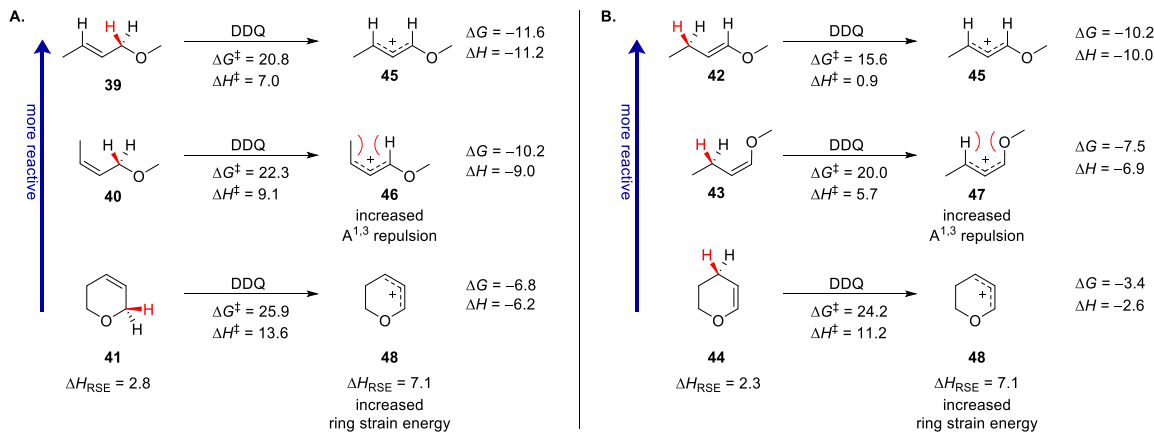


Figure 3. Effects of steric repulsions and ring strain energy on the reactivity of (A) allylic and (B) alkenyl ethers. All energies are in kcal/mol. See SI for details of ring strain energy (ΔH_{RSE}) calculations.

The above discussions clearly indicated the importance of the stability of the carbocation intermediate on the rate of C–H bond cleavage. Nonetheless, a few notable outliners indicate that other factors also contribute to the observed reactivity trend. The reactions of alkenyl ether 13 and allylic ether *trans-15* generate the same oxocarbenium ion after the hydride transfer (Scheme 2d). Thus, the hydride transfer from 13 should be less exergonic than that from 15 because of the greater thermodynamic stability of alkenyl ethers relative to allylic ethers. However, 13 reacts much faster. Here, the reactivity trend is opposite to the thermodynamic driving force of hydride transfer. These experimental observations are confirmed by the DFT calculations shown in Figure 3. The hydride transfer from the alkenyl ether 42 has much lower activation energy than that from the allylic ether 39, despite being less exergonic.

The relationship between the activation energy and the reaction energy of the hydride transfer of the substrates discussed above is illustrated in Figure 4. Within each type of substrate (benzylic, allylic, or alkenyl ethers), a good correlation was obtained – the more stable carbocation leads to a lower activation energy. When comparing different types of substrates, alkenyl ethers are substantially more reactive than the other two types of substrates if the reaction energy to form the carbocation is comparable. Thus, the stability of the carbocation itself is not adequate for establishing a generally applicable model for reactivity. These results prompted us to perform a detailed analysis on the origin of the increased reactivity of alkenyl ethers and to reveal other factors that affect the reactivity of the DDQ-mediated C–H bond cleavage.

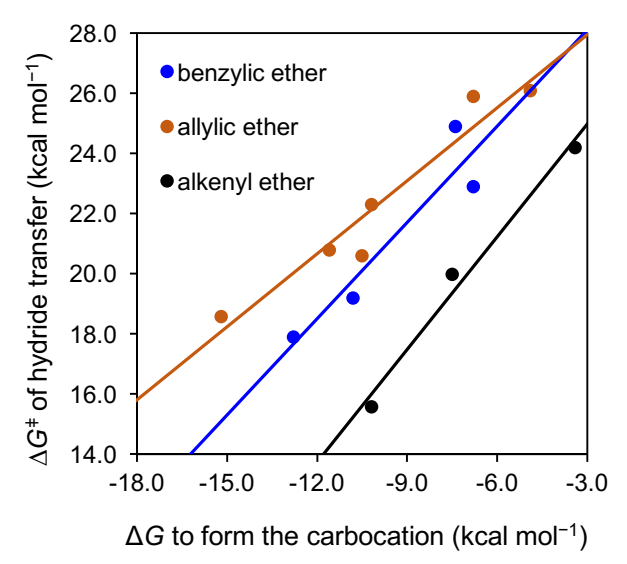


Figure 4. Activation energies (ΔG^{\dagger}) and reaction energies (ΔG) of hydride transfer with three different types of substrates.

3.4. Origin of the Increased Reactivity of Alkenyl Ethers

Several factors may stabilize the hydride transfer transition states and thus increase the reactivity of alkenyl ethers, including electrostatic attraction 27 and secondary orbital interactions 28 between DDQ and the substrate. We performed a detailed computational analysis on these possible factors in the O- and C-attack transition states with alkenyl ether **42** and allyllic ether **39** (Figure 5). Distortion/interaction energy analysis 29 indicates the hydride transfer transition states with alkenyl ether (**TS7** and **TS9**) are stabilized by the stronger interaction energy 30 between DDQ and the alkenyl ether ($\Delta E_{\rm int} = -30.6$ and -40.1 kcal/mol in **TS7** and **TS9**, respectively). In contrast, the interaction energies between DDQ and the allylic ether in **TS8** and **TS10** are significantly smaller (-18.5 and -30.9 kcal/mol, respectively). 31

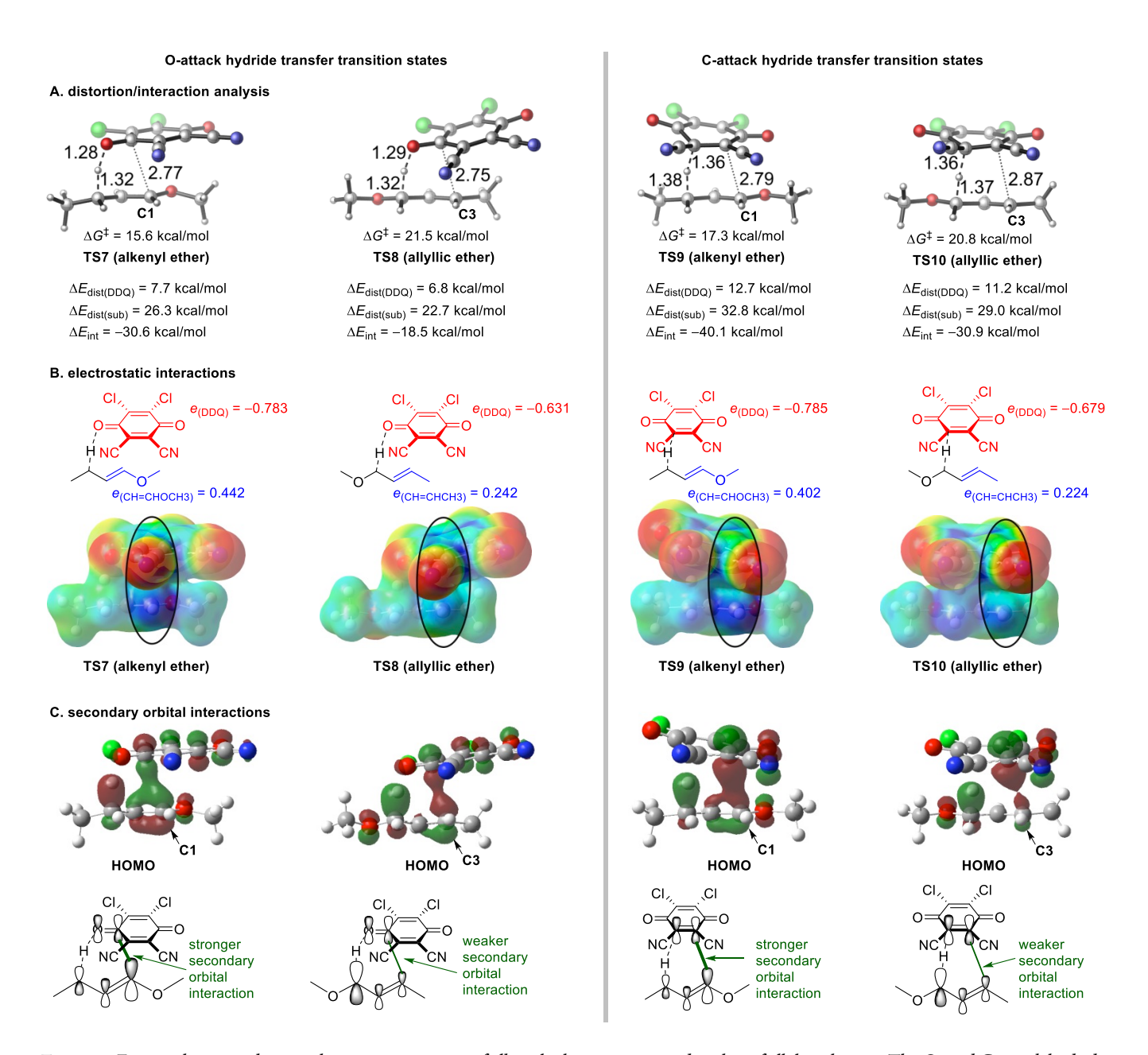


Figure 5. Factors that contribute to the greater reactivity of alkenyl ether **42** compared to that of allylic ether **39**. The O- and C-attack hydride transfer transition states with **42** are stabilized by greater electrostatic attraction and secondary orbital interactions between the DDQ and the substrate. The HOMO of the transition states were generated using the HF/3-21G level of theory.

The difference in interaction energies with the two different substrates is mostly attributed to the through-space interactions between DDQ and the substrate in the hydride transfer transition state. Significant electron transfer from the substrate to DDQ is observed in all of the hydride transfer transition states. The negative charge on DDQ and the positive charge on the substrate lead to strong electrostatic attraction in the transition states. In fact, the quinone ring in DDQ always aligns above the C=C double bond in the substrate to maximize the electrostatic attractions. NPA charge calculations indicate that the DDQ is more negatively charged in TS7 than in TS8 and the double bond moiety in the substrate is more positively charged in TS7 (Figure 5B). Thus, the greater amount of substrate-to-DDQ electron transfer promotes the electrostatic attraction in TS7. Similar electrostatic interactions provide greater stabilization to TS9 than TS10. These electrostatic

interactions are visualized in the electrostatic potential (ESP) surfaces of the transition states. The circled and highlighted region on the ESP surfaces indicate the attractive interactions between DDQ (red, indicating negative potential that attracts positive charge) and the double bond in the substrate (blue, indicating positive potential that attracts negative charge). The darker blue in **TS7** and **TS9** indicates these double bonds are more positively charged and have stronger electrostatic attraction with the DDQ, in agreement with the NPA population analysis.

Examination of the frontier molecular orbitals in the hydride transfer transition states (**TS7-TS10**) revealed moderate secondary orbital interactions between the HOMO of the allylic system and the π^* orbital of C=O or C=C bond on the DDQ (Figure 5C). These secondary donor-acceptor interactions are a result of the relatively short distance between the terminal allylic carbon on the alkenyl and

allylic ethers and the carbonyl carbon or the cyano-substituted carbon on the DDQ (ca. 2.8 Å). In the reaction with alkenyl ethers (TS7), the HOMO of the alkenyl ethers is polarized in a way that there is a larger lobe on C1. This allows better secondary orbital interactions between the HOMO of the alkenyl ethers and the π^* orbital of the C=O bond on DDQ, as indicated by the large HOMO orbital coefficients on C1 in TS7 (Figure 5C). In contrast, in the reaction with the allylic ether substrate, the lobe on C3 is smaller, and thus, a weaker secondary orbital interaction is expected with the π^* orbital of the C=O bond on DDQ. Similar effects also render slightly more favorable secondary orbital interactions in the C-attack TS with alkenyl ether (**TS9**) than with allylic ether (**TS10**). In the reaction with benzylic ethers, the secondary orbital interactions with the π^* orbital on DDQ are less prominent due to the weaker donor ability of the phenyl π orbital (see SI for details). Thus, secondary orbital interactions are not expected to affect the reactivity of benzylic ether substrates.

3.5. Establishing a Predictive Model for Reactivity

The above computational studies revealed two main factors that determine the reactivity of the DDQ-mediated C-H cleavage: the stability of the carbocation intermediate and the extent of electron transfer in the transition state. This creates the possibility for determining whether a mathematical relationship can be established to predict rates based on readily determined molecular properties, in analogy to Sigman's elegant use of multidimensional analytical approaches to gain greater prognosticative capacity for reaction outcomes.³⁴ Here, insights from the DFT studies about the reactivity-determining factors were utilized to rationalize the choice of descriptors for the mathematical model. The extent of electron transfer in the transition state is related to the oxidation potential of the substrate $(E_{1/2}^0, \text{ eq. } 1)$. ³⁵ The stability of carbocation intermediate is related to the hydride dissociation energy of the corresponding C-H bond in solution (ΔG_{HDE} , eq. 2). Both quantities can be easily computed using DFT, 19,24 and are used as parameters for the mathematical relationship for reactivity of the hydride transfer.36

$$RH_{(sol)} \rightarrow RH^{\dagger \bullet}_{(sol)} + e^{-} \qquad E^{0}_{1/2} \tag{1}$$

$$RH_{(sol)} \rightarrow R^{+}_{(sol)} + H^{-}_{(sol)} \Delta G_{HDE}$$
 (2)

Using reactions shown in Table 1 and Figure 3 as the training set, a linear free energy relationship (eq. 3) was established to predict ΔG^{\dagger} values from the hydride dissociation energies (ΔG_{HDE} , kcal/mol) and the oxidation potentials ($E^0_{1/2}$, V vs SCE) of the substrate. It should be noted that only the barriers of the most favorable hydride transfer pathway (either O- or C-attack) were used to train mathematical relationship.

$$\Delta G_{\text{predicted}}^{\ddagger} = 0.485 \ \Delta G_{\text{HDE}} + 4.73 \ E_{1/2}^{0} - 27.7$$
 (3)

Comparing the ΔG^{\dagger} values predicted from this relationship to the DFT-calculated values (Figure 6) shows a good correlation for benzylic, allylic, and alkenyl ethers over a wide range of oxidation potentials ($R^2 = 0.784$). The only outlier from this plot is alkenyl ether 42, which has a lower ΔG^{\dagger} value than predicted. The outlier indicates that other factors, such as secondary orbital interactions in the case of 42, play a role in determining ΔG^{\dagger} . The proximity of DDQ and the substrate in the transition states indicates that sterically hindered alkenes and arenes will undergo carbocation

formation more slowly than expected, as previously reported.^{3c} However, the relationship in eq. 3 proves to be an excellent model for predicting transition state energies in a broad range of reactions and is consistent with experimental observations regarding the importance of oxidation potential and carbocation intermediate stability on reactivity.

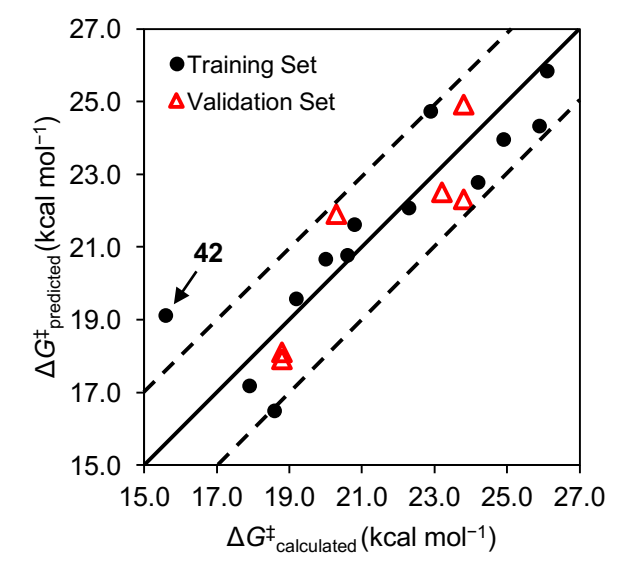


Figure 6. Comparison of hydride transfer activation energies from DFT transition state calculations ($\Delta G^{\dagger}_{\text{calculated}}$) and activation energies predicted from the mathematical relationship using eq. 3 ($\Delta G^{\dagger}_{\text{predicted}}$). Training set: reactions in Table 1 and Figure 3. Validation set: reactions in Table 2.

With the quantitative reactivity model in hand, we next applied eq. 3 to a new set of substrates to validate the applicability of this mathematical relationship. We calculated the hydride dissociation energies and the oxidation potentials of a series of benzylic ether substrates shown in Table 2 and used eq. 3 to derive the predicted Gibbs free energy of activation ($\Delta G^{\dagger}_{\text{predicted}}$). The predicted ΔG^{\dagger} values reliably reproduced the experimental reactivity trend of these substrates.3a For example, although meta-methoxy substitution slightly destabilizes the carbocation (entries 1 vs 2, 3 vs 4), benzylic ethers 50 and 52 are still highly reactive in hydride transfer due to their low oxidation potentials. The moderate reactivities of 2-furanyl ether 53 and 1-naphthyl ether 54 are attributed to their relatively high hydride dissociation energies, although furanyl and naphthyl groups lower the oxidation potentials. Finally, the hydride transfer transition states with 49-54 were calculated using DFT. The DFTcalculated activation energies ($\Delta G^{\dagger}_{calculated}$) are in good agreement with the predicted ΔG^{\dagger} values using eq. 3 (see "validation set" in Figure 6). These validation results suggest that the mathematical relationship (eq. 3) can be applied to predict activation energies of a broad range of substrates with an uncertainty less than 2 kcal/mol and to explain the origin of experimentally observed reactivity trend.

The significance of these studies lies in the ability of the dual dependence of cation stability and oxidation potential on the rate of C–H bond cleavage to explain several other observations that we did not directly investigate in the present study. The enhanced rate of enamides and vinyl sulfides relative to allylic amides and sulfides, ^{3e,f} for example, further illustrates the role of oxidation potential on the activation barrier. The disparate reactivities of enolsilanes in carbocycles, where nucleophilic addition occurs, ³⁷ and heterocycles,

where C–H bond cleavage dominates, ^{6e,f} illustrate the importance of cation stability on the reaction pathway. The facile oxidation of transiently generated enamines to form α,β -unsaturated iminium ions ^{4g} demonstrates the role of both factors. The consistency of these results with theory strongly suggests that this simple analysis provides a powerful predictive tool for understanding the rates of DDQ-mediated reactions for a broad substrate scope.

Table 2. Further Validation of the Mathematical Relationship for Reactivity of the DDQ-Mediated C-H Cleavage

$$\begin{array}{c} \text{OAc} \\ \text{H} \\ \text{Ar} \\ \text{O} \\ \text{C}_6 \text{H}_{13} \end{array} \begin{array}{c} \text{DDQ, DCE} \\ \text{2,6-dichloropyridine} \\ \text{Ar} \\ \text{O} \\ \text{C}_6 \text{H}_{13} \end{array}$$

| entry | substrate ^a | $E^{0}_{1/2}{}^{b}$ | $\Delta G_{	ext{HDE}}^c$ | $\Delta G^{\dagger}_{ m predicted}{}^d$ | $\Delta G^{\dagger}_{ m calculated}{}^{e}$ | | yield (%) ^f |
|-------|------------------------|---------------------|--------------------------|---|--|------|---------------------------|
| 1 | 49 | 2.11 | 88.0 | 24.9 | 23.8 | 14 | 63 |
| 2 | MeO HOONE SO | | 89.2 | 22.3 | 23.8 | 1.5 | 57 |
| 3 | MeO 51 | 1.45 | 80.2 | 18.1 | 18.8 | 0.75 | 74 |
| 4 | MeO 52 | 1.21 | 82.2 | 17.9 | 18.8 | 0.1 | 83 |
| 5 | 53 | 1.73 | 86.6 | 22.5 | 23.2 | 12 | 63 |
| 6 | F-0 54 | 1.60 | 86.6 | 21.9 | 20.3 | 4 | 84 |

^a Methyl ethers (R = Me) were used in the calculations to reduce computational time. ^b Oxidation potential (in V vs SCE) calculated from eq. 1. ^c Hydride dissociation free energy in solution (in kcal/mol) calculated from eq. 2. ^d Predicted ΔG^{\dagger} (in kcal/mol) calculated from eq. 3. ^c Activation free energy of hydride transfer (in kcal/mol) from DFT calculations of O-and C-attack transition states. Only the barrier of the most favorable hydride transfer pathway is shown. ^f Experimental reaction time and yield from Ref. 3a.

4. Conclusion

We employed a computational approach to establish a predictive model for reactivity in the DDQ-mediated C-H bond functionalization of a wide variety of benzylic, allylic, and alkenyl ether substrates. The mathematical model is based on insights from a thorough investigation of the mechanisms of the C-H bond cleavage and factors that affect the stability of the hydride transfer transition states. DFT calculations were performed to reveal that the most favorable mechanism of the C-H cleavage is through a concerted hydride transfer from the substrate to DDQ. Two competing pathways, in which the hydride is transferred to the oxygen and the carbon atoms on DDQ, respectively, have

comparable activation barriers in reactions with benzylic, allylic, and alkenyl ether substrates, in contrast to previous mechanistic studies of the 1,4-cyclohexadiene dehydrogenation that support the O-attack hydride transfer pathway. These mechanistic studies indicate both the C- and O-attack hydride transfer transition states need to be considered in the reaction barrier calculations.

Using DFT calculations, we then identified two key factors that contribute to the reactivity of hydride transfer: (1) the stability of the carbocation intermediate, which could be affected by electronic, steric effects, and ring strain energies, and (2) the electrostatic attraction between DDQ and the substrate in the hydride transfer transition state, which magnitude is affected by the amount of charge transfer in the TS. In addition, secondary orbital interactions between the π orbital of the forming allylic cation and the LUMO of DDQ further stabilize the hydride transfer transition state with alkenyl ether substrates. Based on these mechanistic insights, two parameters that describe the electronic properties of the substrates were chosen to establish a mathematical relationship to quantitatively predict the rate of the C-H cleavage. The hydride dissociation energy in solution (ΔG_{HDE}) describes the stability of the carbocation and the oxidation potential $(E^0_{1/2})$ of the substrate is a competent parameter to describe the magnitude of charge transfer stabilization in the transition state. This mathematical relationship confirmed that the rate of hydride transfer is sensitive to both factors. This model was applied to efficiently predict activation free energies of the hydride transfer and to explain the experimentally observed reactivity trend of a wide variety of substrates.

ASSOCIATED CONTENT

Supporting Information

The Supporting Information is available free of charge on the ACS Publications website.

Computational details and Cartesian coordinates (PDF).

AUTHOR INFORMATION

Corresponding Author

- * florean@pitt.edu
- * pengliu@pitt.edu

Notes

The authors declare no competing financial interests.

ACKNOWLEDGMENT

We thank the NSF (CHE-1654122 for P. L. and CHE-1362396 for P. E. F.) for funding. This material is based upon work supported by the National Science Foundation Graduate Research Fellowship Program under Grant No. 1247842. Calculations were performed at the Center for Research Computing at the University of Pittsburgh and the Extreme Science and Engineering Discovery Environment (XSEDE) supported by NSF.

- NEI ENLINCES
- ¹ For recent reviews on functionalization of aliphatic carbon-hydrogen bonds, see: (a) Liu, L.; Floreancig, P. E. Curr. Opin. Drug Discovery Dev. 2010, 13, 733. (b) Gutekunst, W. R.; Baran, P. S. Chem. Soc. Rev. 2011, 40, 1976. (c) Davies, H. M. L. Angew. Chem., Int. Ed. 2006, 45, 6422. (d) Li, C.-J. Acc. Chem. Res. 2009, 42, 335. (e) Robertson, J.; Pillai, J.; Lush, R. K. Chem. Soc. Rev. 2001, 30, 94.
- ² (a) Walker, D.; Hiebert, J. D. Chem. Rev. **1967**, 67, 153. (b) Buckle, D. R. In Encyclopedia of Reagents for Organic Synthesis; Paquette, L. A., Ed.; John Wiley & Sons: Chichester, UK, **1995**; Vol. 3, p 1699. (c) Wendlandt, A. E.; Stahl, S. S. Angew. Chem. Int. Ed. **2015**, 54, 14638.
- ³ (a) Tu, W.; Liu, L.; Floreancig, P. E. Angew. Chem., Int. Ed. **2008**, 47, 4184. (b) Liu, L.; Floreancig, P. E. Org. Lett. **2009**, 11, 3152. (c) Liu, L.; Floreancig, P. E. Angew. Chem., Int. Ed. **2010**, 49, 3069. (d) Liu, L.; Floreancig, P. E. Angew. Chem., Int. Ed. **2010**, 49, 5894. (e) Brizgys, G. J.; Jung, H. H.; Floreancig, P. E. Chem. Sci. **2012**, 3, 438. (f) Cui, Y.; Floreancig, P. E. Org. Lett. **2012**, 14, 1720. (g) Clausen, D. C.; Floreancig, P. E. J. Org. Chem. **2012**, 77, 6574.
- ⁴ (a) Hayashi, Y.; Mukaiyama, T. Chem. Lett. 1987, 16, 1811. (b) Zhang, Y.; Li, C.-J. Angew. Chem., Int. Ed. 2006, 45, 1949. (c) Zhang, Y.; Li, C.-J. J. Am. Chem. Soc. 2006, 128, 4242. (d) Benfatti, F.; Capdevila, M. G.; Zoli, L.; Benedetto, E.; Cozzi, P. G. Chem. Commun. 2009, 5919. (e) Yu, B.; Jiang, T.; Su, Y.; Pan, X.; She, X. Org. Lett. 2009, 11, 3442. (f) Tsang, A. S.-K.; Jensen, P.; Hook, J. M.; Hashmi, A. S. K.; Todd, M. H. Pure Appl. Chem. 2011, 83, 655. (g) Hayashi, Y.; Itoh, T.; Ishikawa, H. Angew. Chem., Int. Ed. 2011, 50, 3920. (h) Park, S. J.; Price, J. R.; Todd, M. H. J. Org. Chem. 2012, 77, 949. (i) Reddy, B. V. S.; Borkar, P.; Yadav, J. S.; Reddy, P. P.; Kunwar, A. C.; Sridhar, B.; Gree, R. Org. Biomol. Chem. 2012, 10, 1349. (j) Meng, Z.; Sun, S.; Yuan, H.; Lou, H.; Liu, L. Angew. Chem., Int. Ed. 2014, 53, S43. (k) Grenning, A. J.; Snyder, J. K.; Porco, J. A., Jr. Org. Lett. 2014, 16, 792. (l) Wang, H.; Zhao, Y.-L.; Li, L.; Liu, Q. Adv. Synth. Catal. 2014, 356, 3157. (m) Cheng, D.; Wu, L.; Lv, H.; Xu, X.; Yan, J. J. Org. Chem. 2017, 82, 1610. (n) Fradette, R. J.; Kang, M.; West, F. G. Angew. Chem., Int. Ed. 2017, 56, 6335.
- ⁵ (a) Cardillo, C.; Cricchio, R.; Merlin, L., *Tetrahedron* **1971**, 27, 1875. (b) Fu, L.; Yao, C.-J.; Chang, N.-J.; Chen, J.-R.; Lu, J.-R.; Xiao, W.-J. *Org. Biomol. Chem.* **2012**, 10, 506. (c) Yi, H.; Liu, Q.; Liu, J.; Zeng, Z.; Yang, Y.; Lei, A. *ChemSusChem* **2012**, 5, 2143. (d) Lemercier, B. C.; Pierce, J. G. *Org. Lett.* **2015**, 17, 4542.
- (a) Xu, Y.-C.; Kohlman, D. T.; Liang S. X.; Erikkson C. Org. Lett. 1999, 1, 1599.
 (b) Tu, W.; Floreancig, P. E. Angew. Chem., Int. Ed. 2009, 48, 4567. (c) Ghosh, A. K.; Cheng, X. Org. Lett. 2011, 13, 4108. (d) Son, Y. W.; Kwon, T. H.; Lee, J. K.; Rae, A. N.; Lee, J. Y.; Cho, Y. S.; Min, S.-J. Org. Lett. 2011, 13, 6500. (e) Peh, G. R.; Floreancig, P. E. Org. Lett. 2012, 14, 5614. (f) Han, X.; Floreancig, P. E. Angew. Chem., Int. Ed. 2014, 53, 11075. (g) Lu, Z.; Yang, M.; Chen, P.; Xiong, X.; Li, A. Angew. Chem., Int. Ed. 2014, 53, 13840. (h) Jiao, Z.-W.; Tu, Y.-Q.; Zhang, Q.; Liu, W.-X.; Wang, S.-H.; Wang, M. Org. Chem. Front. 2015, 2, 913. (i) Hubert, J. G.; Furkert, D. P.; Brimble, M. A. J. Org. Chem. 2015, 80, 2715. (j) Jiao, Z.-W.; Tu, Y.-Q.; Zhang, Q.; Liu, W.-X.; Zhang, S.-Y.; Wang, S.-H. Zhang, F.-M.; Jiang, S. Nat. Commun. 2015, 6, 7332. (k) Kim, H.; Lee, D. Synlett 2015, 26, 2583.
- 7 Liu, L. Synthesis of Structurally and Stereochemically Diverse Tetrahydropyran Structures via DDQ-Mediated Oxidative Carbon-Hydrogen Bond Activation. Ph.D. Thesis, the University of Pittsburgh, March 2011.
- ⁸ Shehap, O.R; Mansour, A. M. J. Mol. Struct. 2013, 1047, 121.
- ⁹ Turek, A. K.; Hardee, D. J.; Ullman, A. M.; Nocera, D. G.; Jacobsen, E. N. *Angew. Chem. Int. Ed.* **2016**, 55, 539.
- ¹⁰ (a) The reductive potential of DDQ is 0.50 V vs SCE in MeCN. Scribner, R. M. *J. Org. Chem.* **1966**, *31*, 3671. (b) The oxidation potentials of benzylic and allylic ethers are typically within 1.4~2.2 V vs SCE. See SI for oxidation potentials of various benzylic and allylic ethers calculated using DFT. (c) Roth, H. G.; Romero, N. A.; Nicewicz, D. A. *Synlett* **2016**, *27*, 714.
- ¹¹ (a) Hoïler, C.; Ruïchardt, C. Liebigs Ann. 1996, 183. (b) Ruïchardt, C.; Gerst, M.; Ebenhoch, J. Angew. Chem. Int. Ed. Engl. 1997, 36, 1406. (c) Wurche, F.; Sicking, W.; Sustmann, R.; Klärner, F.-G.; Ruïchardt, C. Chem. Eur. J. 2004, 10, 2707.
- 12 Pratt, D. A.; Wright, J. S.; Ingold, K. U. J. Am. Chem. Soc. 1999, 121, 4877.
- ¹³ Jung, H. H.; Floreancig, P. E. Tetrahedron **2009**, 65, 10830.
- ¹⁴ (a) Braude, E. A.; Jackman, L. M.; Linstead, R. P. J. Chem. Soc. **1954**, 3548. (b) Braude, E. A.; Jackman, L. M.; Linstead, R. P. J. Chem. Soc. **1954**, 3564.
- 15 Guo, X.; Zipse, H.; Mayr, H. J. Am. Chem. Soc., 2014, 136, 13863.
- 16 Chan, B.; Radom, L. J. Phys. Chem. A 2007, 111, 6456.

- ¹⁷ (a) Luca, O. R.; Wang, T.; Konezny, S. J.; Batista, V. S.; Crabtree, R. H. New J. Chem., **2011**, 35, 998. (b) Batista, V. S.; Crabtree, R. H.; Konezny, S. J.; Luca, O. R.; Praetorius, J. M. New J. Chem., **2012**, 36, 1141.
- ¹⁸ Yamabe, S.; Yamazaki, S.; Sakaki, S. Int. J. Quantum Chem., 2015, 115, 1533-1542.
- ¹⁹ (a) Würthwein, E. U.; Lang, G.; Schappele, L. H.; Mayr, H. J. Am. Chem. Soc., **2002**, 124, 4084. (b) Shi, J.; Huang, X. Y.; Wang, H. J.; Fu, Y. J. Chem. Inf. Model., **2012**, 52, 63.
- ²⁰ Frisch, M. J.; Trucks, G. W.; Schlegel, H. B.; Scuseria, G. E.; Robb, M. A.; Cheeseman, J. R.; Scalmani, G.; Barone, V.; Mennucci, B.; Petersson, G. A.; Nakatsuji, H.; Caricato, M.; Li, X.; Hratchian, H. P.; Izmaylov, A. F.; Bloino, J.; Zheng, G.; Sonnenberg, J. L.; Hada, M.; Ehara, M.; Toyota, K.; Fukuda, R.; Hasegawa, J.; Ishida, M.; Nakajima, T.; Honda, Y.; Kitao, O.; Nakai, H.; Vreven, T.; Montgomery, J. A., Jr.; Peralta, J. E.; Ogliaro, F.; Bearpark, M.; Heyd, J. J.; Brothers, E.; Kudin, K. N.; Staroverov, V. N.; Kobayashi, R.; Normand, J.; Raghavachari, K.; Rendell, A.; Burant, J. C.; Iyengar, S. S.; Tomasi, J.; Cossi, M.; Rega, N.; Millam, N. J.; Klene, M.; Knox, J. E.; Cross, J. B.; Bakken, V.; Adamo, C.; Jaramillo, J.; Gomperts, R.; Stratmann, R. E.; Yazyev, O.; Austin, A. J.; Cammi, R.; Pomelli, C.; Ochterski, J. W.; Martin, R. L.; Morokuma, K.; Zakrzewski, V. G.; Voth, G. A.; Salvador, P.; Dannenberg, J. J.; Dapprich, S.; Daniels, A. D.; Farkas, O.; Foresman, J. B.; Ortiz, J. V.; Cioslowski, J.; Fox, D. J. Gaussian 09, Revision D.01; Gaussian, Inc.: Wallingford, CT, 2009
- ²¹ CYLview, 1.0b; Legault, C. Y. Universitéde Sherbrooke: Quebec, Canada, (2009); http://www.cylview.org
- ²² Zhao, Y.; Truhlar, D. G. Theor. Chem. Acc. 2008, 120, 215.
- Marenich, A. V.; Cramer, C. J.; Truhlar, D. G. J. Phys. Chem. B, 2009, 113, 6378.
 (a) Winget, P.; Cramer, C. J.; Truhlar, D. G. Theor. Chem. Acc., 2004, 112, 217.
 (b) Isse, A. A.; Lin, C. Y.; Coote, M. L.; Gennaro, A. J. Phys. Chem. B, 2011, 115, 678.
 (c) Huynh, M. T.; Anson, C. W.; Cavell, A. C.; Stahl, S. S.; Hammes-Schiffer,
- ²⁵ Marcus, R. A. J. Chem. Phys. 1956, 24, 966.

S. J. Am. Chem. Soc. 2016, 138, 15903.

- ²⁶ These results are in accord with previous computational studies from Chan and Radom (ref. 16), which suggested the closed-shell ionic pathway is favored in polar solvents.
- ²⁷ (a) Wu, Y. D.; Tucker, J. A.; Houk, K. N. *J. Am. Chem. Soc.* **1991**, *113*, 5018. (b) Paddonrow, M. N.; Wu, Y. D.; Houk, K. N. *J. Am. Chem. Soc.* **1992**, *114*, 10638. (c) Liu, P.; Yang, X.; Birman, V. B.; Houk, K. N. *Org. Lett.*, **2012**, *14*, 3288.
- ²⁸ (a) Hoffmann, R.; Woodward, R. B. J. Am. Chem. Soc. **1965**, 87, 4388. (b) Levandowski, B. J.; Houk, K. N. J. Am. Chem. Soc. **2016**, 138, 16731.
- ²⁹ (a) Bickelhaupt, F. M.; Houk, K. N. Angew. Chem. Int. Ed. 2017, 56, 10070. (b) Ess, D. H.; Houk, K. N. J. Am. Chem. Soc. 2008, 130, 10187.
- 30 The interaction energy was calculated using the following equation: $\Delta E_{\rm int} = E_{\rm TS} E_{\rm sub(TS)} E_{\rm DDQ(TS)}$, according to the procedure reported in Ref. 29b. Here, $E_{\rm TS}$ is the electronic energy of the transition state structure; $E_{\rm sub(TS)}$ and $E_{\rm DDQ(TS)}$ are the electronic energies of the substrate and the DDQ fragments at their transition state geometries.
- ³¹ The C-attack transition states have greater interaction energies than the O-attack transition states because the more endothermic C-attack pathway has later transition states, as evidenced by the longer C–H distances in **TS9** and **TS10** compared to those in **TS7** and **TS8**.
- 32 The through-bond interaction energies in **TS7** and **TS8** are expected to be similar due to the similar forming O–H distances in these transition states. Similarly, the through-bond interactions in the forming C–H bond in **TS9** and **TS10** are also expected to be similar.
- ³³ The importance of contact between the DDQ and the alkene moiety is consistent with the lower reactivity of vinylsilanes (ref. 3c), which are more sterically congested to achieve the stacked geometry for the electrostatic attractions.
- ³⁴ Sigman, M. S.; Harper, K. C.; Bess, E. N.; Milo, A. Acc. Chem. Res., 2016, 49, 1292.
- 35 A moderate correlation between the oxidation potential $(E^0_{1/2})$ of the substrate and the amount of charge transfer in the hydride transfer transition state was observed for the hydride transfer reactions in Table 1 and Figure 3. See SI for details.
- ³⁶ For examples of using redox potentials as parameters for linear free energy relationship: (a) Edwards, J. O. *J. Am. Chem. Soc.* **1954**, *6*, 1540. (b) Edwards, J. O. *J. Am. Chem. Soc.* **1956**, 78, 1819. (c) Sevov, C. S.; Hickey, D. P.; Cook, M. E.;

Robinson, S. G.; Barnett, S.; Minteer, S. D.; Sigman, M. S.; Sanford, M. S. J. Am. Chem. Soc. 2017, 139, 1452.

³⁷ (a) Guo, X.; Mayr, H. J. Am. Chem. Soc. 2013, 135, 12377. (b) Ryu, I.; Murai, S.; Hatayama, Y.; Sonoda, N. Tetrahedron Lett. 1978, 19, 3455 (c) Bhattacharya, A.; DiMichele, L. M.; Dolling, U.-H.; Grabowski, E. J. J.; Grenda, V. J. J. Org. Chem. 1989, 54, 6118. (d) Hodgson, D. M.; Moreno-Clavijo, E.; Day, S. E.; Man, S. Org. Biomol. Chem. 2013, 11, 5362.

TOC Graphic